Ultralight carbon aerogel from nanocellulose as a highly selective oil absorption material

Article *in* Cellulose · February 2015

DOI: 10.1007/s10570-014-0519-5

6 authors, including:

Timothy Mark Young
University of Tennessee
161 PUBLICATIONS **1,573** CITATIONS
SEE PROFILE

Peizhi Liu
Taiyuan University of Technology
56 PUBLICATIONS **872** CITATIONS
SEE PROFILE

Cristian I Contescu
Oak Ridge National Laboratory
150 PUBLICATIONS **3,784** CITATIONS
SEE PROFILE

Cellulose
DOI 10.1007/s10570-014-0519-5

ORIGINAL PAPER

Ultralight carbon aerogel from nanocellulose as a highly selective oil absorption material

Yujie Meng · Timothy M. Young · Peizhi Liu · Cristian I. Contescu · Biao Huang · Siqun Wang

Received: 25 August 2014 / Accepted: 28 November 2014

Abstract The synthesis of a sponge-like carbon aerogel from microfibril cellulose, with high porosity (99 %), ultra-low density (0.01 g/cm^3), hydrophobic properties (149° static contact angle) and reusability is reported in this paper. The physical properties, internal morphology, thermal properties, and chemical properties of carbon aerogels heat-treated at 700 and 900 °C (Samples C-700 and C-900) were examined. Stabilization and carbonization parameters were optimized in terms of residual carbon yield. The BET surface area of Sample C-700 (521 m^2/g) was significantly higher than of Sample C-950 (145 m^2/g). Graphitic-like domains were observed in C-950. The highest normalized sorption capacity (86 g/g) for paraffin oil was observed in sample C-700. The removal of hydrophilic function groups during carbonization causes carbon aerogel to present highly hydrophobic properties. Carbon aerogel's ability to absorb oil is enhanced by its highly porous 3D network structure with interconnected cellulose nanofibrils.

Keywords Nanocellulose · Carbon aerogel · Oil absorption · 3D network structure

Y. Meng · T. M. Young · B. Huang · S. Wang (✉)
Department of Forestry, Wildlife and Fisheries, Center for Renewable Carbon, University of Tennessee, Knoxville, TN, USA
e-mail: swang@utk.edu

P. Liu
Department of Materials Science and Engineering, University of Tennessee, Knoxville, TN, USA

C. I. Contescu
Oak Ridge National Laboratory, Oak Ridge, TN, USA

B. Huang
College of Engineering, Fujian Agriculture and Forestry University, Fuzhou, China

Introduction

Oil spills and oily industrial wastewater are of environmental concern and have economic consequences, driving oil-related industries to look for new and more effective technologies for cleaning up and reclaiming the oil spills. Oil recovery using absorbent materials is superior to many other industrial methods for oil recovery, such as physical collection, biodegradation, or in situ burning, because of the lower costs, higher efficiency and higher recyclability of most absorbents (Hubbe et al. 2013). Although conventional absorbent materials have been widely used for large-scale oil spill cleanup, their absorption efficiency is greatly impaired by the high water affinity of most natural materials (Peng et al. 2013). In contrast, absorbents from natural precursors with both hydrophobic and oleophilic properties have the potential of being both practically and commercially important.

Nanocellulose has attracted scientific and practical interest relatively recently not only because of its bio-

Published online: 04 December 2014

based, sustainable, nontoxic, abundant, and renewable nature, but because of its unique intrinsic properties (Dong et al. 2013). In particular, microfibril cellulose (MFC) consists of long, flexible fibers cleaved from the hierarchy of plant or wood cellulose by mechanical processes (Cheng et al. 2007; Moon et al. 2011; Wang and Cheng 2009). The high surface area and high aspect ratio of MFC are beneficial for the formation of an ultrafine three-dimensional network structures in an aqueous environment. As a consequence, attention has turned towards converting natural cellulose nanofibrils into cellulose aerogels with low density, high porosity, and low thermal conductivity, as needed for various applications (Cervin et al. 2012; Chen et al. 2011; Hoepfner et al. 2008; Jin et al. 2011; Li et al. 2011). The hydrophilic property of nanocellulose aerogel resulting from its molecular structure is an obvious limitation on its capacity for water–oil separation. Surface functionalization and conversion by pyrolysis into carbon aerogel provide ways to overcome this difficulty (Dong et al. 2013; Jin et al. 2011; Korhonen et al. 2011; Liu et al. 2013). It has been reported that graphene aerogel, carbon nanotube aerogel, carbon fiber aerogel, and carbon microbelts aerogel are capable of separating water and oil (Gui et al. 2011; Hu et al. 2013; Li et al. 2010, 2014; Upadhyayula et al. 2009; Wu et al. 2013). However, these materials are not necessarily environmentally or economically desirable because they are obtained either by means of complex syntheses that require large amounts of chemical reagents, or through high-energy input processes.

This paper reports on the synthesis and properties of sponge-like bulk materials made from nanocellulose and their potential to effectively absorb oil. The main point is that, using a nanoscale material as a precursor allows thermal treatment temperatures to be reduced while retaining important properties (porous structure, surface area, hydrophobic properties) that are similar to those of other carbon absorbent materials synthesized from conventional cellulose-based precursors. This study uses a "green" synthesis approach that involves (1) freeze-drying a mixture of MFC and applying wet resin to create a 3D porous aerogel, and (2) thermal treatment to achieve both hydrophobic and oleophilic properties.

In this study, the oil absorption properties of this product are characterized, and the effects of porosity and density differences on the resulting hydrophobic and oleophilic capabilities are investigated. The advantages of this new product are its low cost, its use of renewable and sustainable raw materials, its non-toxicity, and its biodegradability. This ultralight and extremely hydrophobic carbon aerogel can selectively separate and remove large-scale oil spills from water surfaces and can be used potentially for absorbing of a variety of other organic solvents.

Materials and experimental section

Materials

Cellulose microfibrils with a solid content of 10 % were obtained from commercial sources (Celish KY-100G, Daicel Corporation, Japan). Cross-linker KymeneTM resin (Ashland Hercules Inc., USA) was purchased and added into the MFC suspension.

Preparation of MFC aerogel and carbon aerogel

A mixture of 2 wt% aqueous suspension of cellulose microfibril and cross linker resin (5 wt% of dry MFC) was poured into open-ended copper pipes (1.5 inch in length and 0.81 inch in diameter) and sealed with aluminum foil. The samples were then placed into liquid nitrogen for 1 min for rapidly freezing, following which the aluminum foil was removed and the samples were freeze-dried in a vacuum lyophilizer (Labconco, Inc., Kansas City, MO) at −51 °C for 3 days. Ultra-light sponge-like aerogel was obtained. Samples were oven-heated at 120 °C for 3 h to promote cross-linking in order to form a three-dimensional network. The aerogel samples were stabilized in air (20 mL/min) and carbonized in nitrogen (20 mL/min) using a Lindberg/blue M Mini-Mite tube furnace (Thermo Scientific). The stabilization stage included (1) heating the sample from room temperature to 180 °C at a rate of 10 °C/min in air; (2) increasing the temperature from 180 to 230 °C at a rate of 5 °C/min in air; and (3) increasing the temperature from 230 to 320 °C in air. Different heating rates ranging from 0.2 to 5 °C/min were used in the latter step. The carbonization stage included (4) increasing the temperature from 320 °C to peak temperatures of 700 or 950 °C at a rate of 5 °C/min in nitrogen and holding for 15 min. Samples were then cooled to room temperature. The carbon aerogels were

labeled C-700 and C-950, according to their carbonization temperature.

Characterization of MFC aerogel and carbon aerogel

The bulk density ρ of MFC aerogel and carbon aerogel was calculated using Eq. (1):

$$\rho = m/V \quad (1)$$

where m is the weight and V is the bulk volume. The porosity P of cellulose microfibril aerogel and carbon aerogel were calculated using Eq. (2):

$$P(\%) = (1 - \rho_a/\rho_m) \times 100\% \quad (2)$$

where ρ_a is the bulk density and ρ_m is the skeletal density of MFC and carbon fibers, respectively. The skeletal density was measured by helium ultrapycnometry (Quantachrome Corp, USA). The inner structures of MFC aerogel and carbon aerogel were observed by means of scanning electron microscopy (SEM, Zeiss Auriga SEM/FIB crossbeam workstation, Germany). The MFC aerogel was coated with a thin layer of gold to provide conductivity and to protect the sample from electron beam damage. An ultrastructure of the carbon aerogel was characterized by transmission electron microscopy (TEM, Zeiss Libra 200 MC, Germany). The carbonized aerogel was ground into powder and dispersed into distilled water. TEM samples were prepared by depositing suspension drops (0.001 % w/v in water) on amorphous lacey carbon-coated electron microscope grids and were then allowed to dry. The TEM was operated at a 200 kV accelerating voltage. Thermal stability and carbonization yield were determined using thermogravimetric (TG) analyzers (TGA; Perkin–Elmer 7 series; Perkin–Elmer Cetus Instruments, USA). The heating program was set up to mimic the stabilization/carbonization process. The TGA program for the MFC aerogel sample without stabilization was set at 5 °C/min heating rate from room temperature to peak temperature. Fourier transform infrared spectroscopy (FTIR) was performed on the MFC aerogel and the carbon aerogel using a Perkin Elmer FTIR-ATR spectrometer (Spectrum One, Perkin Elmer, USA). Samples were placed on the diamond crystal of an attenuated total reflectance (ATR) accessory. All spectra were collected over the range of 4,000–600 cm^{-1} at 4 cm^{-1} resolution with 16 scans. The static contact angle was measured on the carbonized aerogels at room temperature using the sessile drop method. Changes of contacted angle were measured and recorded by using a JC2000A contact angle meter (Shanghai Zhongchen Digital Technology and Equipment Co., Shanghai, China). A droplet of deionized water was deposited by a syringe, which pointed vertically down onto the surface of the carbon aerogels. A high-resolution camera sequentially recorded the droplet images on the surface as a function of time. The contacted angle was measured by goniometer. Nitrogen adsorption-desorption analysis of the carbon aerogels was carried out on an Autosorb 1C instrument (Quantachrome Instruments, USA). The Brunauer–Emmett–Teller (BET) surface area (m^2/g) was calculated from the nitrogen adsorption data at 77 K in a relative pressure range from 0.05 to 0.35. The pore size distribution was calculated by the non-local density functional theory (NLDFT) from the adsorption branch of the isotherm. The mass percent of elements (carbon, hydrogen and nitrogen) in the MFC aerogel and the carbon aerogel were determined by a 2400 Series II CHNS/O elemental analyzer (PerkinElmer, USA).

Oil sorption experiments

Oil sorption experiments were carried out using canola oil (Wesson, ConAgra Foods, Inc.), diesel oil (BP PLC gas station), paraffin oil (BP PLC gas station) and pump oil (motor oil, Castrol North America Inc.). Carbon aerogel sponges that had been heat-treated at two peak temperatures (700 and 950 °C) were weighed first and immersed into oil for variable times, totaling 1,600 s. After each immersion, the sponge was taken out, drained for 30 s to wipe away the excess oil, and immediately transferred to a tarred pan. The process was repeated and thus the weight increase rate of carbon aerogel was measured as a function of time. Sorption kinetics were analyzed and calculated as the ratio of oil absorbed to dry absorbent weight (ASTM F726, standard method of testing sorbent performance of absorbents E1-1993):

$$Q_t = (m_{st} - m_o)/m_o \quad (3)$$

where Q_t is the oil absorbency, m_{st} is the weight of carbon aerogel at time t of oil tests and m_o is the initial dry weight of carbon aerogel. The oil absorbency ratio

by weight was plotted as a function of time. After the carbon aerogels reached sorption saturation, the samples were immersed into ethanol to completely remove the absorbed oil, oven-dried at 60 °C overnight, weighted, and reused for subsequent absorption testing. The reusability of the carbon aerogel on oil absorption was verified over 10 cycles.

Results and discussion

Thermal decomposition kinetics

The oxidative stabilization and carbonization behavior of MFC aerogel was studied by TGA. TG and derivative thermogravimetric (DTG) thermograms are shown in Fig. 1. The carbon yield of MFC aerogel without stabilization (6.2 %) was found to be significantly lower than that of samples with stabilization treatment.

Oxidative stabilization was performed to promote cross-linking and avoid "melting" or shrinkage of MFC aerogel. Three regions of weight loss at different temperature ranges were seen. A barely detectable weight loss occurred between 105 and 230 °C. A rapid mass loss process started from 230 °C and terminated at 320 °C, with the sample residual mass between 15 and 20 %. During the oxidative stabilization process, it has been found that the splitting of glycosidic bonds in cellulose's macromolecular chains leads to the formation of a large number of oxygenated compounds (Tang and Bacon 1964). Therefore, in order to achieve a high char yield, attention was given to the rapid mass loss processes. It was found that the heating rate has a considerable influence on the mass loss between 230 and 320 °C. The onset of degradation temperatures and the weight loss of carbonized aerogel under different heating rates are summarized in Table 1. The onset and decomposition temperatures of stabilized MFC aerogels increased with the increase in the heating rate. Because decomposition is triggered by temperature and limited by the diffusion of gases from the MFC mass, decomposition started earlier when the samples were subjected to low heating rates than it did at high heating rates. This "thermal inertia" effect is common to TGA experiments when the sample comes slowly into equilibrium with the external furnace temperature. A slow weight loss occurred between 320 and 950 °C after the gas was switched to nitrogen. The final carbon yield was 9–14 % of initial weight. Fifty-five percent of the weight loss was attributed to the removal of hydrogen and oxygen in cellulosic material according to the reaction formula (Wu et al. 2008). However, more weight loss was detected from the TGA analysis and was attributed to carbon loss as CO and CO_2 during depolymerization and scission. It has been shown that the heating rate plays an important role in the char

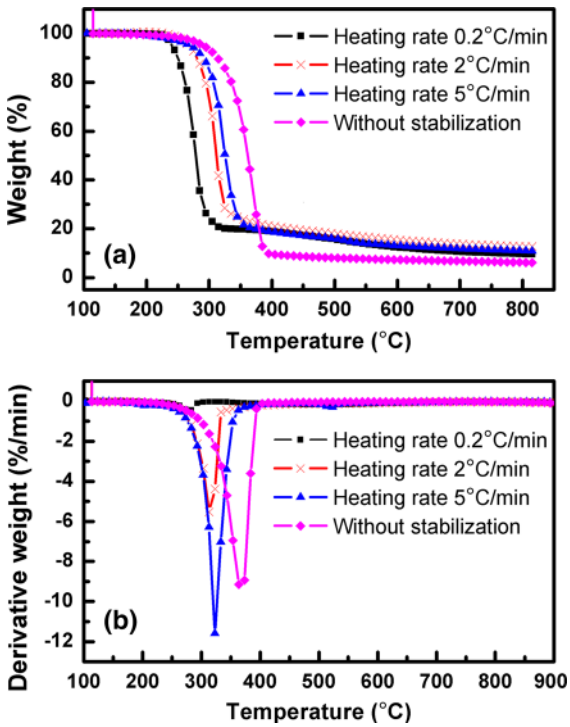

Fig. 1 Thermogravimetric analysis (TGA) curves showing the effect of heating rate during the temperature rising from 230 to 320 °C on carbon residual yield at 800 °C **a** TGA curves, **b** DTG curves

Table 1 Onset temperature, degradation temperature and weight loss of MFC aerogel under different heating rates

Heating rate (°C/min)	Onset temperature (°C)	Degradation temperature (°C)	Weight loss (%)
0.2	256.28	279.77	90.36
2	293.26	215.29	86.02
5	306.12	323.02	89.04
Without stabilization treatment	334.63	368.65	93.85

yield during cellulose carbonization (Milosavljevic and Suuberg 1995).

The effect of the heating rate during the rapid mass loss processes (230–320 °C) on the char yield at 800 °C was also compared. The char yield increased significantly when the heating rate increased from 0.2 to 2 °C/min. At this latter heating rate, the char yield was 14 %. When heating rates were set faster than 2 °C/min, a slight trend toward lower char yield was observed. Compared to macroscopic fibers such as cotton, the MFC began to decompose at a significantly lower temperature due to the larger surface area that was exposed to heat, dramatically cutting the energy input and allowing a lower heating temperature during carbonization for making the porous material (Gaspar et al. 2014).

Structure of MFC aerogel and carbon aerogel

The structure of an absorbent material has a strong influence on its oil absorption capacity. In the most favorable conditions for aerogel preparation, the volume of carbon aerogel shrinks to 13 % of that of MFC aerogel, while the weight of carbon aerogel drops to 6 % of MFC aerogel. The bulk density of MFC aerogel is 0.025 g/cm^3, decreasing to 0.010 g/cm^3 after carbonization. Skeletal density of MFC aerogel is 1.48 g/cm^3; 1.4 g/cm^3 for carbon aerogel C-950; and 1.33 g/cm^3 for carbon aerogel C-700. Figure 2 shows SEM images of MFC aerogel and carbon aerogel C-950. Both types of aerogel consist of a 3D network structure with interconnected microfibrils in which large spaces are present among the entangled fibers. Pore sizes span a range between tens of nanometers and tens of micrometers. The morphology of MFC aerogel and carbon aerogel differ in that the fiber diameter of MFC aerogel is from 50 to 200 nm, and that of carbon aerogel is from 10 to 20 nm. Cellulose fibrils shrink considerably during carbonization because of the removal of non-carbon elements. The Kymene^{TM} resin (PEA) starts to crosslink in the process of heating and acts on the points where fibers intersect to facilitate the formation of a three-dimensional structure because the amino chlorohydrin and azetidinium chloride (ring) groups existent in PEA resin have the ability to react with carboxyl groups on the cellulose surface, which helps to bonding adjacent fibers (Fig. 3). FTIR spectra of MFC raw material and crosslinked MFC aerogel are presented in Fig. 4. The ratio of peak intensity at 1,650 cm^{-1} (amide C=O stretch) to the peak intensity at 1,043 cm^{-1} (C–O stretch) increases dramatically after crosslinking, indicating the reaction between cellulose and the crosslinker (Zhang et al. 2012). TEM images of Sample C-950 show well-developed graphitic-like domains composed of about 20 parallel fringes as well as numerous uncorrelated fragments. The (002) fringes originate from the graphene sheets and extend perpendicularly to the image plane. Figure 2f shows the electron diffraction pattern of Sample C-950 corresponding to image 2e, which confirms the presence of graphitic stacks. The graphitic structure was barely observed, however, in Sample C-700.

Surface area and porosity of carbon aerogels

According to formula (2), the porosity was calculated at 97.8 % for the MFC aerogel and 99 % for the two carbon aerogels. Nitrogen adsorption at 77 K detects micropores, comparable with the diameter of N_2 molecules, and mesopores where capillary condensation N_2 occurs. The larger micrometer-size voids in the aerogel structure (Fig. 2d) were not measured by this method, so the porosity information obtained from gas adsorption on these aerogels was limited to micropores (<20 Å) and mesopores (20–500 Å). On these very open materials, multilayer adsorption of nitrogen occurs freely on the external surface of fibers and ligaments visible in the SEM images. The BET equation provides a reliable measurement of the total surface area in these materials (Brunauer et al. 1938).

Adsorption isotherms of nitrogen at 77 K on Samples C-700 and C-950 are shown in Fig. 5. Both samples yielded IUPAC Type II isotherms at 77 K, indicating that a mixture of micropores and open surface is present in the carbon aerogel on which unrestricted monolayer-multilayer adsorption occurs (Ryu et al. 1999). Sharp inflection points are present at a low relative pressure of about 0.1, showing the transition from micropore filling to multilayer adsorption. The slow isotherm rise that follows next indicates multilayer adsorption of nitrogen on the exposed surface of the 3D fibrous network in carbon aerogels (Fig. 2d). This exposed surface makes the major contribution to oil absorption, rather than micropores or mesopores.

Sample C-700 showed a higher N_2 uptake than Sample C-950 did. The BET surface area of carbon aerogel C-700 (521 m^2/g in Table 2) was in range with

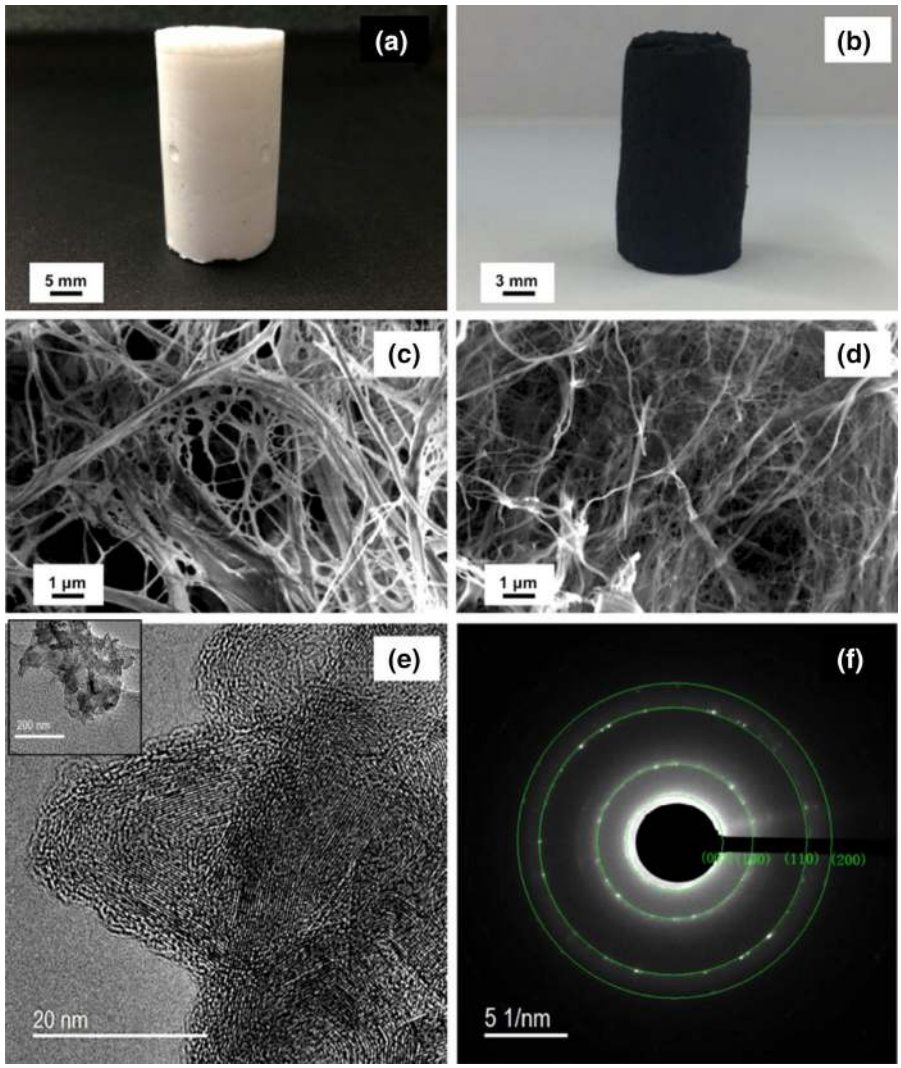

Fig. 2 Photographs of **a** microfibril cellulose aerogel, and **b** carbon aerogel (C-950); SEM images of **c** microfibril cellulose aerogel, and **d** carbon aerogel (C-950); TEM images of **e** graphitic domains in the structure of carbon aerogel C-950 and **f** diffraction pattern from the same carbon aerogel

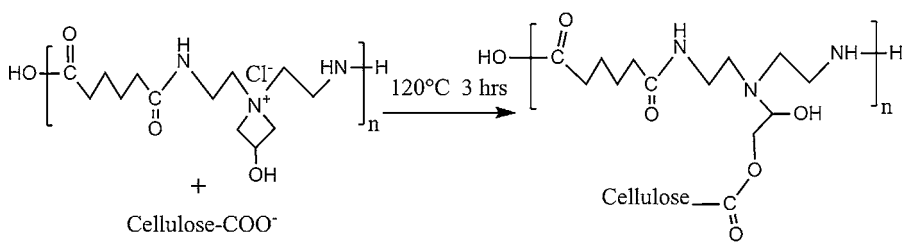

Fig. 3 The formation of ester bond between Kymene™ crosslinker and cellulose carboxyl groups

other reported results (Kipling et al. 1964). However, the surface area of C-950 was found to be only 145 m^2/g, lower than the 449 m^2/g reported for a carbon prepared from pure cellulose at a peak temperature of 1,000 °C (Xie et al. 2009). This is attributable to the formation of graphite-like domains observed in the HR-TEM images of Sample C-950. It is reasonable to assume that more carbon sheets were

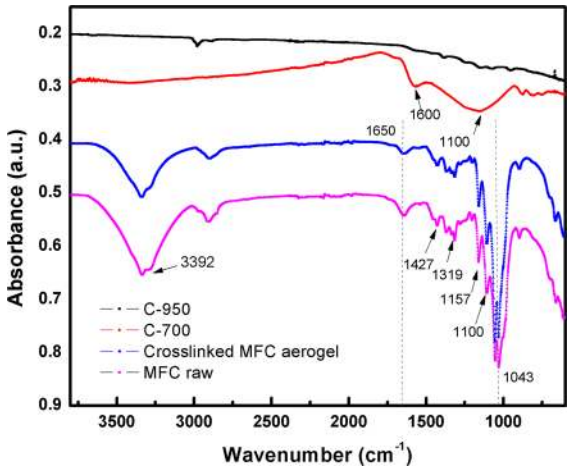

Fig. 4 FTIR spectra of MFC aerogel and carbon aerogels

tightly stacked in Sample C-950 than in Sample C-700, which would eliminate the voids among the formed graphene sheets and would reduce the total surface area. The difference in BET surface area values explains why Sample C-700 had higher oil absorption capacity compared to Sample C-950 for the same oil type. Figure 5b shows the distribution of internal surface area versus pore sizes for the two carbon aerogel samples, obtained by the NLDFT method. A majority of the surface area measured by nitrogen adsorption was contained in micropores (<20 Å) and lower mesopores (20–200 Å). The same information was obtained from Fig. 5c, d, where the differential and cumulative pore size distributions were calculated by the NLDFT method. The total pore volume for pores up to 300 Å was larger for Sample

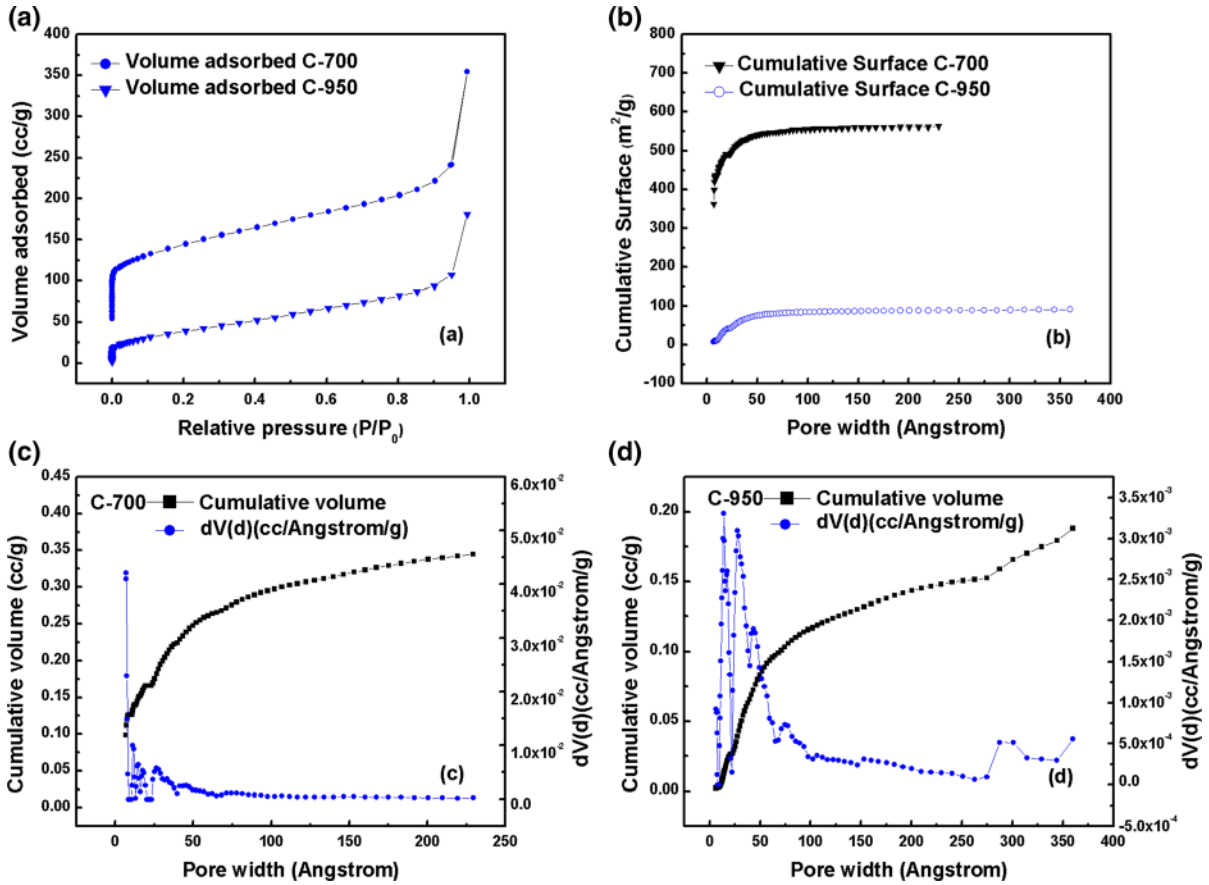

Fig. 5 **a** Adsorption isotherms of nitrogen on carbon aerogel heat-treated at 700 and 950 °C; **b** cumulative surface distribution of carbon aerogels and **c**, **d** differential and cumulative pore size distributions determined by NLDFT method for Samples C-700 (**c**) C-950 (**d**)

Table 2 Carbon aerogel's properties and fitting parameters of the sorption kinetics

Sample ID	Porosity (%)		Sponge density (g/cm^3)		BET surface area (m^2/g)	
	99		0.01		145	
	Pollutants	Pollutants density (g/cm^3)	Viscosity (cST)	K ($\times 10^{-3}$ s^{-1})	N-Q_s (g/g)	T_h (s)
C-950	Canola oil	0.890	70	4.6	65.9	3.7
	Diesel oil	0.772	10	36.9	58.4	0.6
	Paraffin oil	0.758	6	20.0	66.2	1.0
	Pump oil	0.888	250	3.08	50.0	7.2
C-700	Canola oil	0.890	70	4.9	73.6	3.2
	Diesel oil	0.772	10	32.4	72.8	0.6
	Paraffin oil	0.758	6	21.1	86.6	0.9
	Pump oil	0.888	250	3.64	55.8	4.7

N-Q_s is the normalized saturated sorption capacity in terms of oil density; t_h is time when carbon aerogel reaches one-half of the saturated sorption capacity

C-700 (0.55 cm^3/g) than for Sample C-950 (0.28 cm^3/g), in agreement with the values of the BET surface area. Micropores (<2 nm) were seen to represent a small fraction of the pore volume measured by gas adsorption (30 % in C-700; 9 % in C-950). Supermicropores (0.7–2 nm) were present on both samples, although in an extremely low amount, on Sample C-950 and in larger proportions on Sample C-700. More significant was the fraction of lower mesopores (up to about 20 nm) on both samples.

Hydrophobic properties of carbon aerogel surface

The wetting properties of MFC aerogel and carbon aerogel were further investigated by static contact angle measurement. When water droplets were dropped on the MFC aerogel surface, the droplets spread out and were taken up immediately by the porous sponge, indicating a low contact angle. This hydrophilic character is associated with the presence of hydrophilic surface groups on the MFC aerogel surface. FTIR spectra of MFC aerogel showed dominant peaks at 1,043, 3,392, 1,640, and 1,160 cm^{-1}, which were identified as C–O, –OH, C=O, C–O–C, respectively (Fig. 4). Pyrolysis changed the water behavior uptake of the carbonized aerogels significantly, making them strongly hydrophobic. Figure 6 shows the behavior of water droplets on the surface of carbonized aerogel C-950 and the evolution of the contact angle. Despite a slight decrease with time (from 149° to 144°), the contact angle at the water/carbonized aerogel boundary remained very high, indicating a strong hydrophobic character. FTIR

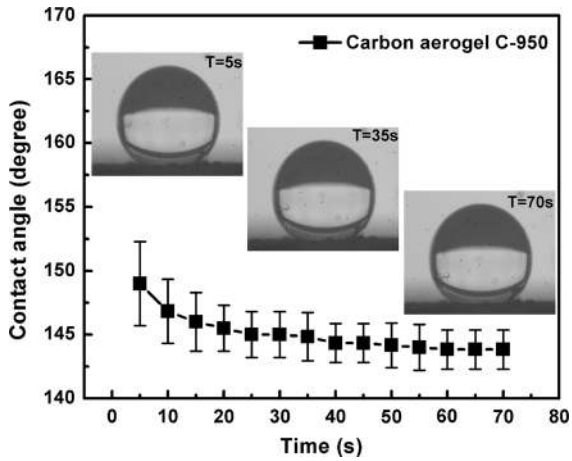

Fig. 6 Carbon aerogel wetting characterization by static contact angle analysis

analysis confirmed the absence of hydrophilic groups; the remaining FTIR bands still visibly (Fig. 4) correspond to aromatic carbon bonds, which cause the hydrophobic characteristic. Interestingly, the FTIR spectrum of Sample C-700 shows peaks at 1,600 and 1,100 cm^{-1} corresponding to the C=C and C–N stretch. Nitrogen was seen to be present in large amounts in the PEA resin as indicated by the elemental analysis, amounting to about 2 wt% in MFC aerogel and increasing to about 3.3 % in both carbonized aerogel samples. Carbonization causes a strong increase in carbon content and a drop in hydrogen content (Table 3). The experimental characterization reported above demonstrates the water-repellent and oleophilic properties of carbon aerogel. Thus, this ultralight, high porous material is able to effectively

clean oil spills by selectively absorbing oil floating on water, a finding that is of great significance for practical applications.

Oil absorption

An oil absorption test using four representative oils was conducted for the purpose of verifying the oil sorption kinetics of carbon aerogels and their oil storage capacity. Figure 7a–c, sequential photographs, show that a piece of carbon absorbs blue engine oil in a few seconds. The sorption kinetic action is presented in Fig. 8a–d, where the oil absorbency was plotted against sorption time. These results provide two important pieces of information. First, visible observation showed that the carbon aerogel was rapidly wetted at the very beginning of absorption. Data collected at initial absorption times exhibited a very high sorption rate, indicating the capillary rise. The oil then penetrated into the pores by capillary action. Secondly, diffusion was observed later in the sorption curve, as shown by a slow step during the oil absorption process. On all four types of oils, Sample C-700 demonstrated higher oil absorption capacity than did Sample C-950. The absorption capacities, normalized by dividing the weight gain into oil

Table 3 Elemental percentage of MFC aerogel as an average of 2 runs before and after carbonization

Sample	Weight (mg)	Average Weight (%)			O
		C	N	H	
MFC aerogel	2.1	43.55	2.15	6.26	48.04
C-700	2.1	81.59	3.30	1.62	13.49
C-950	2.3	84.78	3.39	0.88	10.95

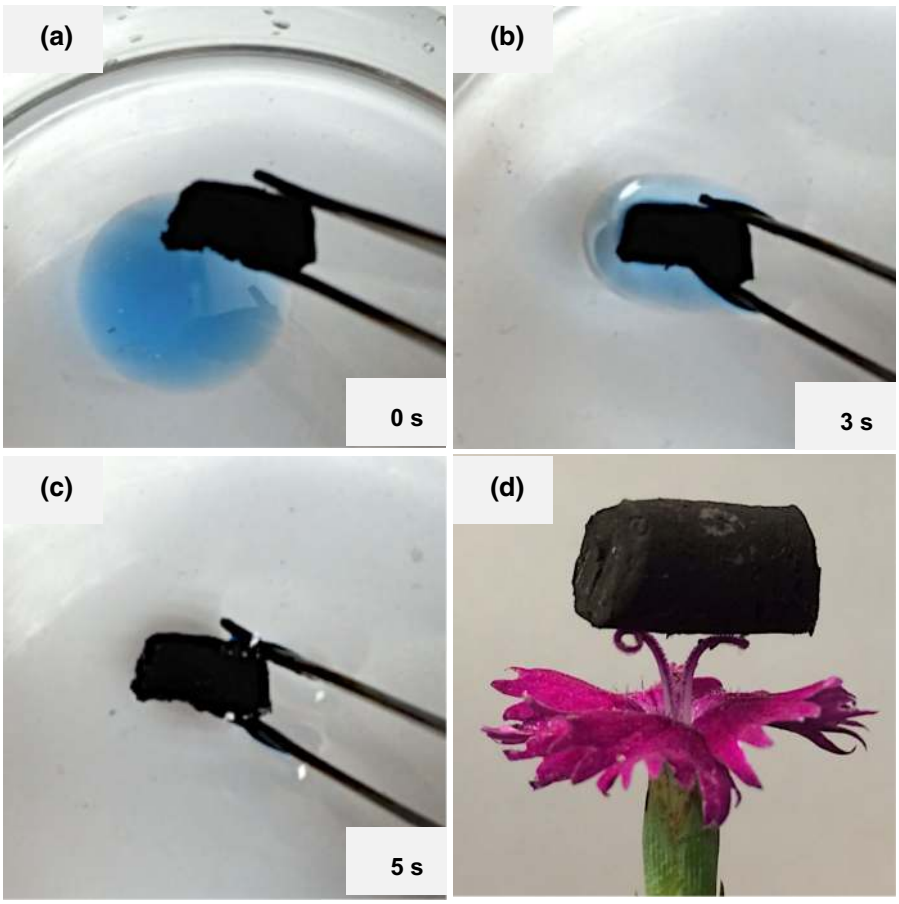

Fig. 7 **a–c** Removal of engine oil from the water surface using nanocellulose carbon aerogel. **d** Ultralight carbon aerogel sitting on a flower

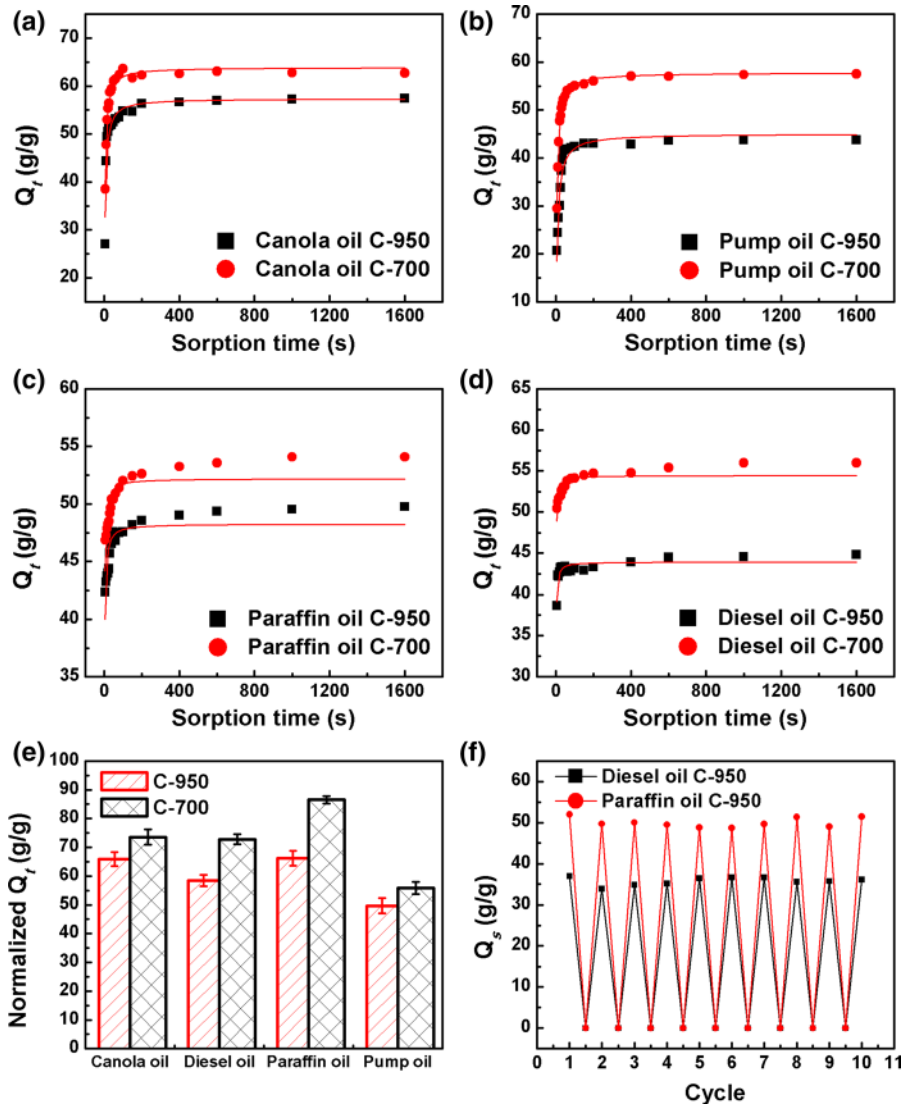

Fig. 8 Sorption kinetics of different oils absorbed by carbonized MFC aerogel: **a** canola oil, **b** pump oil, **c** diesel oil, **d** paraffin oil, **e** normalized saturated sorption capacities of different oils by oil density, **f** absorption reusability of carbon aerogel

density, are shown in Fig. 8e. Sample C-700 had the highest normalized saturated oil absorption capacity (87 times its own weight) for paraffin oil. It takes longer for carbon aerogel to reach one-half the saturated sorption capacity with high viscosity oil. It is evident that the same oil diffused faster on Sample C-700 than on Sample C-950. An important implication of these findings is that lower-temperature pyrolysis of MFC aerogel is to be preferred for preparation of oil absorbent materials with higher absorption capacity.

The sorption kinetics of carbon aerogel was analyzed based on the following pseudo-second order model and equation (Bastani et al. 2006; Gui et al. 2011):

$$\frac{1}{(Q_s - Q_t)} = \frac{1}{Q_s} + kt \tag{4}$$

where Q_s is saturated oil absorption, Q_t is the oil absorbed at time t and k is the kinetic rate constant. The red lines plotted in Fig. 8 show the fitting results of four different oils, and Table 2 summarizes the fitting parameters. The predicted results correlated well to the experimental data.

The analysis of porosity and SEM images provides information on the structure of carbon aerogel. Capillary

condensation and excess adsorption are believed to dominate the carbon aerogels' properties during absorption. The structure and the volume of carbon aerogel dominate the oil storage amount, while the number of capillaries dominates the absorption rate. Given its ultra-low density and its high open porosity, carbon aerogel has a significantly higher oil absorbency Q_s when compared to other oil absorbents such as TiO_2/nanocellulose aerogel ($Q_s = 27$ for paraffin), winter melon carbon aerogel ($Q_s = 26$ for diesel), cotton towel ($Q_s = 5$ for diesel), cellulase modified corn stalk ($Q_s = 16.6$ for diesel), PU sponge ($Q_s = 42$ for diesel), graphite/isobutylene-isoprene aerogel ($Q_s = 22$ for diesel) and swellable porous PDMS ($Q_s = 12$ for diesel) etc. (Choi et al. 2011; Li et al. 2014; Peng et al. 2013; Zhang et al. 2013). The time for carbon aerogel to reach one-half of the saturated sorption capacity, denoted as t_h, was used to characterize the absorption rate. The t_h value for diesel absorption ($t_h = 0.6$ s) was the smallest among the four different oils, indicating a very fast absorption rate. Because oil density and viscosity play important roles in the absorption capacity of carbon aerogel, the normalized oil absorption capacity of carbon aerogel for paraffin oil ranks the highest among the four kinds of oils. The oil density also contributes to the saturated absorption capacity in carbon aerogels with same pore size distribution and 3D network structure. Despite the fact that Sample C-950 has low BET surface area (145 m^2/g), it still achieved much higher absorption capacity compared to other absorbents. This indicates that macropores and the open pore structure make the carbon aerogel a very efficient oil absorbent. The large pores created by the 3D network structure should provide better accessibility for oil or organic solvent molecules. On the contrary, on absorbent materials that are mainly dominated by micropores and mesopores, highly viscous oil is potentially retarded by viscous drag, which prevents the oil from permeating when being absorbed. Most organic solvents and oils have small surface free tension, usually in the range of 20–30 mJ/m^2 (pump oil 28.21 mJ/m^2, diesel oil 24.14 mJ/m^2). However, carbon fibers' surface free energy is 40–50 mJ/m^2, which is close to that of oil but smaller than the surface free tension of water (72.8 mJ/m^2) (Harkins and Brown 1919). This makes it easy for oil to infiltrate the pores of carbon aerogel. Thus, the water-repelling and oil-wetting properties qualify carbon aerogel as a perfect absorbent candidate for oil-water separation.

To verify the reusability of carbon aerogel for oil removal, the oil sorption experiments were repeated after the oil-soaked samples were thoroughly cleaned in ethanol and dried. As Fig. 8f shows, the carbon aerogel was found to retain the same oil absorption capacity after ten absorption/desorption cycles.

Conclusions

This paper reports on the synthesis and properties of a sponge-like nanocellulose-based carbon aerogel. This material is useful as a highly porous oil absorbent (99 % porosity) with ultralight density (0.01 g/cm^3), hydrophobic properties (149° static contact angel), fast absorption rate, and multiple reusability. The carbon aerogel material was obtained through heat treatment of cellulose microfibril aerogel. The heating rate during the rapid mass loss process in the carbonization stage was optimized to 2 °C/min to achieve high carbon yield. The structure-adsorption properties relationships of carbon aerogel were demonstrated. Carbon aerogel heat-treated at 700 °C was found to possess higher oil absorption capacity of various types of oils, correlating with its higher BET surface area (521 m^2/g), compared to the carbon aerogel heat-treated at 950 °C (145 m^2/g). The factor mainly responsible for the high oil-absorption capacity is the 3D network structure formed by the entanglement of carbonized cellulose fibrils and the large surface energy of carbonized fibers, and micropores enhance the absorption capacity to some extent. These unique properties of carbon aerogel, along with the advantages of using a natural, renewable, low-cost, and sustainable material, recommend carbon aerogel treated in this way for a wide range of oil-spill cleanup applications.

Acknowledgments The authors gratefully acknowledge financial support from the UTIA 2013 Innovation Grant and the US Forest Service Southern Research Station under contract agreement 07-CR-11330115-087, Southeastern Sun Grant Center. CIC acknowledges support for materials characterization from the US Department of Energy, Basic Energy Sciences, Materials Science and Technology Division.

References

Bastani D, Safekordi AA, Alihosseini A, Taghikhani V (2006) Study of oil sorption by expanded perlite at 298.15 k. Sep Purif Technol 52:295–300. doi:10.1016/j.seppur.2006.05.004

Brunauer S, Emmett PH, Teller E (1938) Adsorption of gases in multimolecular layers. J Am Chem Soc 60:309–319. doi:10.1021/ja01269a023

Cervin NT, Aulin C, Larsson PT, Wagberg L (2012) Ultra porous nanocellulose aerogels as separation medium for mixtures of oil/water liquids. Cellulose 19:401–410. doi:10.1007/s10570-011-9629-5

Chen W, Yu H, Li Q, Liu Y, Li J (2011) Ultralight and highly flexible aerogels with long cellulose I nanofibers. Soft Matter 7:10360–10368. doi:10.1039/c1sm06179h

Cheng Q, Wang S, Rials T, Lee S (2007) Physical and mechanical properties of polyvinyl alcohol and polypropylene composite materials reinforced with fibril aggregates isolated from regenerated cellulose fibers. Cellulose 14:593–602. doi:10.1007/s10570-007-9141-0

Choi S-J, Kwon T-H, Im H, Moon D-I, Baek DJ, Seol M-L, Duarte JP, Choi Y-K (2011) A polydimethylsiloxane (pdms) sponge for the selective absorption of oil from water. Acs Appl Mater Interfaces 3:4552–4556. doi:10.1021/am201352w

Dong C, Zhang H, Pang Z, Liu Y, Zhang F (2013) Sulfonated modification of cotton linter and its application as adsorbent for high-efficiency removal of lead(II) in effluent. Bioresour Technol 146:512–518. doi:10.1016/j.biortech.2013.07.108

Gaspar D, Fernandes SN, de Oliveira AG, Fernandes JG, Grey P, Pontes RV, Pereira L, Martins R, Godinho MH, Fortunato E (2014) Nanocrystalline cellulose applied simultaneously as the gate dielectric and the substrate in flexible field effect transistors. Nanotechnology 25:094008. doi:10.1088/0957-4484/25/9/094008

Gui X, Li H, Wang K, Wei J, Jia Y, Li Z, Fan L, Cao A, Zhu H, Wu D (2011) Recyclable carbon nanotube sponges for oil absorption. Acta Mater 59:4798–4804. doi:10.1016/j.actamat.2011.04.022

Harkins WD, Brown FE (1919) The determination of surface tension (free surface energy), and the weight of falling drops—the surface tension of water and benzene by the capillary height method. J Am Chem Soc 41:499–524. doi:10.1021/ja01461a003

Hoepfner S, Ratke L, Milow B (2008) Synthesis and characterisation of nanofibrillar cellulose aerogels. Cellulose 15:121–129. doi:10.1007/s10570-007-9146-8

Hu H, Zhao Z, Wan W, Gogotsi Y, Qiu J (2013) Ultralight and highly compressible graphene aerogels. Adv Mater 25:2219–2223. doi:10.1002/adma.201204530

Hubbe MA, Ayoub A, Daystar JS, Venditti RA, Pawlak JJ (2013) Enhanced absorbent products incorporating cellulose and its derivatives: a review. Bioresources 8:6556–6629

Jin H, Kettunen M, Laiho A, Pynnonen H, Paltakari J, Marmur A, Ikkala O, Ras RHA (2011) Superhydrophobic and superoleophobic nanocellulose aerogel membranes as bioinspired cargo carriers on water and oil. Langmuir 27:1930–1934. doi:10.1021/la103877r

Kipling JJ, Sherwood JN, Shooter PV, Thompson NR (1964) The pore structure and surface area of high-temperature polymer carbons. Carbon 1:321–328. doi:10.1016/0008-6223(64)90286-6

Korhonen JT, Kettunen M, Ras RHA, Ikkala O (2011) Hydrophobic nanocellulose aerogels as floating, sustainable, reusable, and recyclable oil absorbents. Acs Appl Mater Interfaces 3:1813–1816. doi:10.1021/am200475b

Li H, Gui X, Zhang L, Wang S, Ji C, Wei J, Wang K, Zhu H, Wu D, Cao A (2010) Carbon nanotube sponge filters for trapping nanoparticles and dye molecules from water. Chem Commun 46:7966–7968. doi:10.1039/c0cc03290e

Li J, Lu Y, Yang D, Sun Q, Liu Y, Zhao H (2011) Lignocellulose aerogel from wood-ionic liquid solution (1-allyl-3-methylimidazolium chloride) under freezing and thawing conditions. Biomacromolecules 12:1860–1867. doi:10.1021/bm200205z

Li Y, Samad YA, Polychronopoulou K, Alhassan SM, Liao K (2014) Carbon aerogel from winter melon for highly efficient and recyclable oils and organic solvents absorption. Acs Sustian Chem Eng 2:1492–1497. doi:10.1021/sc500161b

Liu Y, Ma J, Wu T, Wang X, Huang G, Liu Y, Qiu H, Li Y, Wang W, Gao J (2013) Cost-effective reduced graphene oxide-coated polyurethane sponge as a highly efficient and reusable oil-absorbent. Acs Appl Mater Interfaces 5:10018–10026. doi:10.1021/am4024252

Milosavljevic I, Suuberg EM (1995) Cellulose thermal decomposition kinetics: global mass loss kinetics. Ind Eng Chem Res 34:1081–1091. doi:10.1021/ie00043a009

Moon RJ, Martini A, Nairn J, Simonsen J, Youngblood J (2011) Cellulose nanomaterials review: structure, properties and nanocomposites. Chem Soc Rev 40:3941–3994. doi:10.1039/c0cs00108b

Peng D, Lan Z, Guo C, Yang C, Dang Z (2013) Application of cellulase for the modification of corn stalk: leading to oil sorption. Bioresour Technol 137:414–418. doi:10.1016/j.biortech.2013.03.178

Ryu Z, Zheng J, Wang M, Zhang B (1999) Characterization of pore size distributions on carbonaceous adsorbents by DFT. Carbon 37:1257–1264. doi:10.1016/S0008-6223(98)00322-4

Tang MM, Bacon R (1964) Carbonization of cellulose fibers.1. Low temperature pyrolysis. Carbon 1:390. doi:10.1016/0008-6223(64)90035-1

Upadhyayula VKK, Deng S, Mitchell MC, Smith GB (2009) Application of carbon nanotube technology for removal of contaminants in drinking water: a review. Sci Total Environ 408:1–13. doi:10.1016/j.scitotenv.2009.09.027

Wang S, Cheng Q (2009) A novel process to isolate fibrils from cellulose fibers by high-intensity ultrasonication, part 1: process optimization. J Appl Polym Sci 113:1270–1275. doi:10.1002/app.30072

Wu Q, Pan N, Deng K, Pan D (2008) Thermogravimetry–mass spectrometry on the pyrolysis process of lyocell fibers with and without catalyst. Carbohydr Polym 72:222–228. doi:10.1016/j.carbpol.2007.08.005

Wu Z, Li C, Liang H, Chen J, Yu S (2013) Ultralight, flexible, and fire-resistant carbon nanofiber aerogels from bacterial cellulose. Angew Chem Int Ed Engl 52:2925–2929. doi:10.1002/anie.201209676

Xie X, Goodell B, Zhang D, Nagle DC, Qian Y, Peterson ML, Jellison J (2009) Characterization of carbons derived from cellulose and lignin and their oxidative behavior. Bioresour Technol 100:1797–1802. doi:10.1016/j.biortech.2008.09.057

Zhang W, Zhang Y, Lu C, Deng Y (2012) Aerogels from crosslinked cellulose nano/micro-fibrils and their fast

shape recovery property in water. J Mater Chem 22:11642–11650. doi:10.1039/c2jm30688c

Zhang A, Chen M, Du C, Guo H, Bai H, Li L (2013) Poly(dimethylsiloxane) oil absorbent with a three-dimensionally interconnected porous structure and swellable skeleton. Acs Appl Mater Interfaces 5:10201–10206. doi:10.1021/am4029203